# Deformable Registration of 3D Vessel Structures to a Single Projection Image

Darko Zikic[1], Martin Groher[1], Ali Khamene[2], and Nassir Navab[1]

[1] Computer Aided Medical Procedures (CAMP), Technische Universität München, Germany
[2] Siemens Corporate Research (SCR), Princeton, USA

## ABSTRACT

Alignment of angiographic preoperative 3D scans to intraoperative 2D projections is an important issue for 3D depth perception and navigation during interventions. Currently, in a setting where only one 2D projection is available, methods employing a rigid transformation model present the state of the art for this problem. In this work, we introduce a method capable of deformably registering 3D vessel structures to a respective single projection of the scene. Our approach addresses the inherent ill-posedness of the problem by incorporating a priori knowledge about the vessel structures into the formulation. We minimize the distance between the 2D points and corresponding projected 3D points together with regularization terms encoding the properties of length preservation of vessel structures and smoothness of deformation. We demonstrate the performance and accuracy of the proposed method by quantitative tests on synthetic examples as well as real angiographic scenes.

**Keywords:** Registration, Angiography

## 1. INTRODUCTION

Angiographic imaging is a widely used technique for visualization of vessel anatomy in diagnosis and treatment. During most abdominal catheterizations, contrasted 2D projections from one view are acquired by a C-arm for catheter guidance and treatment monitoring. A 3D angiographic scan - that is, a Computed Tomography Angiography (CTA), or a Magnetic Resonance Angiography (MRA) scan - is usually acquired preoperatively to assess the region of interest and identify possible complications for the treatment. This 2D/3D setting is sketched in Figure 1. In clinical practice, the available 3D information is currently not brought to the interventional room. Only guided by images from one view, it is often very difficult for the physician to find a path through the patient's vessel system mainly due to overlay of vessel structures and breathing deformation.

An accurate registration of 3D to 2D vasculature would yield one-to-one vessel feature correspondences, which can be used for intraoperative 3D roadmapping or catheter tip backprojection. With this 3D enhancement of angiographic interventions, both increase in depth perception and decrease in injected contrast agent can be achieved.

In abdominal or thoracic regions that are subject to deformation, these correspondences cannot be established by a mere rigid or affine transformation model. Instead, it is necessary to create a 3D deformation field that locally deforms the 3D vasculature such that its projection matches the 2D vasculature.

For 3D-3D registration of vascular images, methods have been developed to compute the deformation field from sparse correspondences that are determined manually or through rigid pre-alignment.[1,2] However, the computation of a dense 3D deformation field from sparse 2D-3D feature correspondences is in general an ill-posed problem: The displacement of a point along the projection ray cannot be computed without additional constraints, compare Figures 2 and 3b.

Currently, methods for 2D-3D alignment of vascular images use a rigid transformation model discarding local motion. Such algorithms tend to be robust against deformation changes of vessel structures but do not solve for

Further author information: (Send correspondence to Darko Zikic)
Darko Zikic: E-mail: zikic@in.tum.de
Martin Groher: E-mail: groher@in.tum.de
Ali Khamene: E-mail: ali.khamene@siemens.com
Nassir Navab: E-mail: navab@in.tum.de

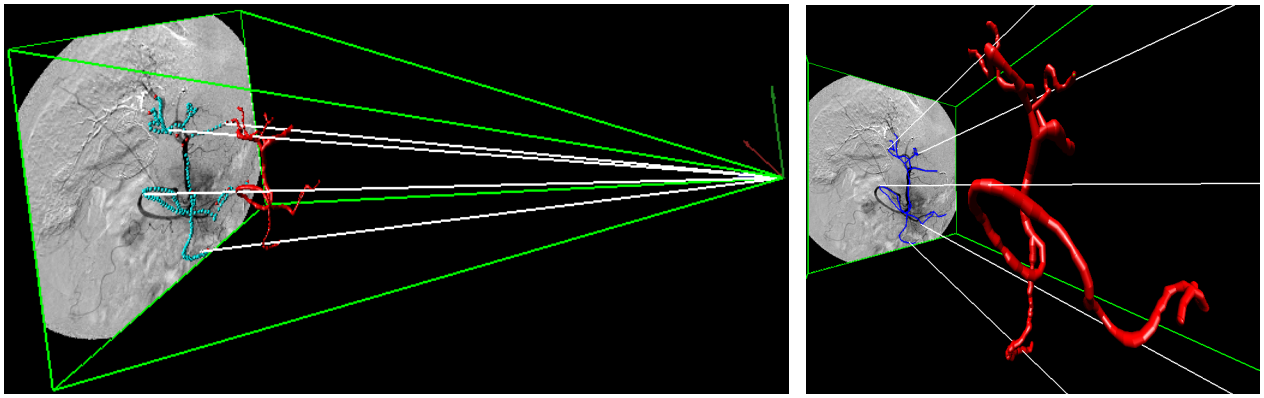

Figure 1: Visualization of the 2D/3D C-arm/patient scenario. The 3D vasculature is to be deformably registered to the 2D projection image. **Upper Image:** The blue line in the 2D Digitally Subtracted Angiogram (DSA) visualizes the projected centerline of the rigidly registered 3D vasculature. This projection is visibly deformed to the projection in the DSA due to breathing motion. **Lower Image:** Overview figure of the projective scene symbolizing the C-arm/patient scenario.

these changes, leaving a considerable amount of misalignment, which can be, as reported for e.g. liver, up to 2 cm.[3]

In order to overcome the shortcomings of the rigid approach, we propose a method for computing a meaningful deformation of a 3D structure from a single 2D projection. Our method combines the correspondence-based approach and the ideas from intensity-based registration, where the registration problem is defined as a minimization of an energy consisting of a difference measure and regularization terms, which incorporate the a priori knowledge about the problem, see Figure 2.

The difference term used in our approach penalizes the distance between the projection of 3D points from the input vasculature, represented as nodes of a centerline graph, and the corresponding points from the 2D projection image (Figure 3a).

Minimizing only the difference term results in what we refer to as the *Naive approach*, which is not able of recovering the deformation in the projection direction and thus leads to unnatural results. In order to be able to compute the 3D displacement, additionally to the difference, we employ a combination of two regularization terms, which model assumptions about vessel structures and thus yield realistic deformations.

The first term describes the assumption that the length of vessels does not change heavily inside the human body and penalizes large changes of the vessel length. This term is important since it presents constraints in 3D space and thus reduces number of solutions for one node from infinite to two along the projection ray, if one of the neighbors is assumed fixed (Figure 3b). Also, in our experiments the minimization of this term results in the nearest solution to the initial position of the respective point. Figure 3a illustrates the idea of using the difference term together with length preservation.

However, for real graphs with many nodes and large deformations the length preservation term has the drawback that the behavior is too local. Although the length preservation itself is successful, in these cases the property that the nearest solution to the initial position is computed introduces unnatural bends in the vessels, thus leading to unwanted results, compare Figure 4. In order to counteract this effect, we impose a smoothness condition on the resulting displacement field. This is done by using the standard diffusion regularization term, compare for example.[4]

Usually, the diffusion regularization term is equipped with a boundary condition (e.g. Dirichlet, where the boundary values are fixed) which restricts the null-space of the term. Fixing certain displacement values would require to have at least one vessel point, for which the position is known. However, selecting such a 3D point in a deforming volume would present a very difficult - if not impossible - task. Thus, we replace the boundary

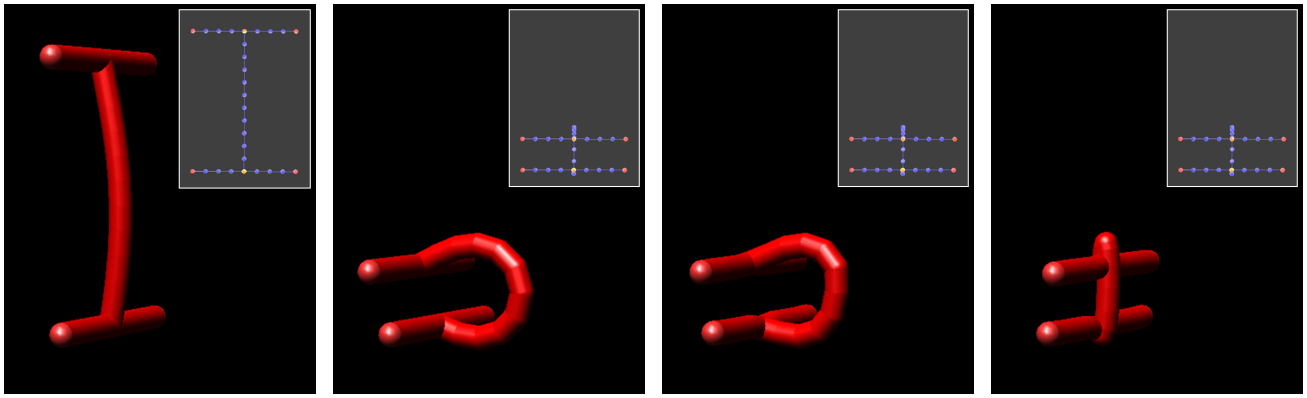

(a) Input 3D image (b) Ground truth (c) Proposed method (d) Naive approach

Figure 2: Visualization of the method results on a simple synthetic example, with the window-in-window presenting the 2D projection of the respective 3D structure. **(a)** is the input 3D graph to be deformed while **(b)** shows a graph, which was used to generate the input 2D projection image. Hence, (b) presents the ground truth for the deformation of (a). The camera is positioned on the right side of the images, such that the shape change in ray direction is not observable from the 2D projection image. **(c)** With the naive approach using only the distance measure from a single projection, it is not possible to recover the full 3D deformation since there are no constraints along the projection rays. **(d)** Employing the length preservation and diffusion regularization terms present additional constraints and thus allows for correct deformation also in the direction along the projection rays.

condition by the soft constraint of position retention, which can easily be integrated into the optimization procedure.

So in summary, our method enables meaningful 3D deformations of 3D vessel structures based on a single 2D projection of the same structure. To the best of our knowledge this is the first time that this problem is addressed in the field of medical image processing.

A short supplementary movie illustrating the proposed algorithm is available at `http://campar.in.tum.de/personal/zikic/spie2008/2d3d_Deformable_XVid.avi`.

### 1.1 Relation to Prior Work

There is a considerable body of research on *rigid* 2D-3D registration of vascular images. These mostly address rigid structures, for example in neuro surgery, see[5–8] and references therein. For the case of abdominal or thoracic 2D-3D image alignment, there exist some methods, which are supplemented by gating information or robustness against deformations.[9–11] However, although robust to local transformations, these methods still use a rigid transformation model and do not account for the occurring deformation.

2D-3D deformable registration on medical images has been addressed by Fleute *et al.* ,[12] Benameur *et al.* ,[13] Yao *et al.* ,[14] Zheng *et al.* ,[15] and Tang *et al.* [16] all within the context of registration of two or more 2D projections to an atlas or statistical model of bone anatomy. These methods do not focus on vessel anatomy and do not cope with a single view scenario.

To our knowledge, there is no work that uses the constraint of length preservation of vessel structures for image registration.

In the robotics and graphic community, computing the 3D pose of a model from a 2D image is regarded as an inverse kinematics problem (see e.g. Grochow *et al.* [17] and references therein), which is somewhat related to our topic. However, the model which is used in these approaches often just has a very limited number of degrees of freedom (DOF) unlike our model, where each feature point introduces 3 DOF.

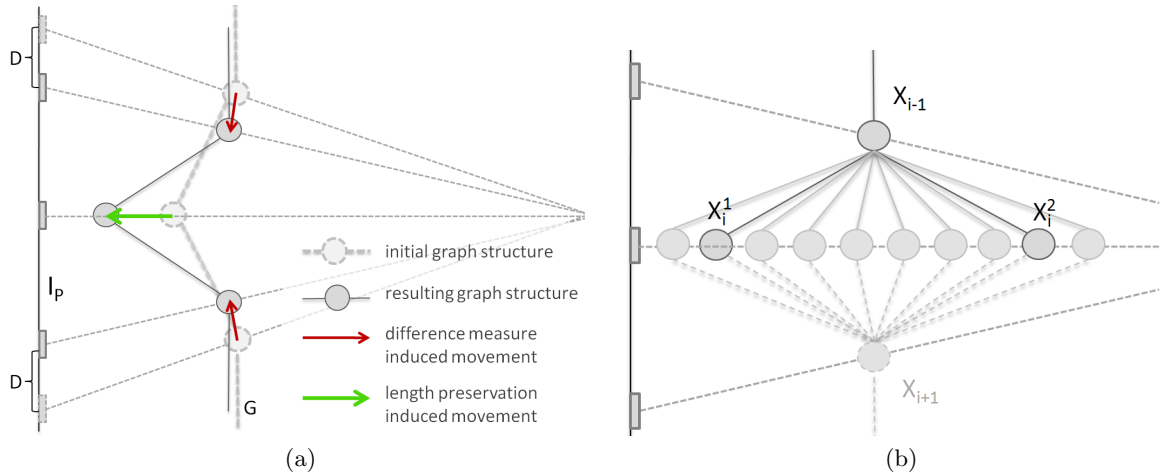


Figure 3: **Left Image (a):** 2D illustration of the effect of the difference measure and the length preservation term on the motion of the vessel structure. The difference term $D$ measures the distance in the 2D projection image $I_p$. The length preservation penalizes the change of length of the 3D graph $G$. **Right Image (b):** Illustrates the reduction of admissible solutions for one node along the projection ray, by using length preservation. For the fixed node $\mathbf{X}_{i-1}$, the position of the node $\mathbf{X}_i$ is constrained to two possible solutions, $\mathbf{X}_i^1$ and $\mathbf{X}_i^2$, if the distance between $\mathbf{X}_{i-1}$ and $\mathbf{X}_i$ is assumed constant.

## 2. METHOD

The basic idea of the proposed method is to use a difference term and supplement it by regularization terms which incorporate a priori knowledge about the problem and thus impose constraints along the projection rays, which are needed in order to render the problem well-posed. Having modeled the problem this way, the solution is computed by using an optimization method of choice. Since the focus of this work is on the modeling part, we use the standard gradient descent optimization scheme.*

In the following, we first briefly describe the setting for the algorithm and the performed pre-processing steps. We go on by presenting notation and introducing structures we use. Then we define the model and in the following subsections we present the single components of the energy function to be optimized.

### 2.1 Setting and Preprocessing

As input for our method we use an extracted model of 2D and 3D vasculature, as well as a feature-based rigid pre-alignment in a calibrated setting† yielding a projection matrix and correspondence information between 2D and 3D feature points. All of these steps have been previously presented in the literature and are not within the scope of this paper. A graph model is created in both 2D and 3D from a region growing step yielding vessel segmentations, followed by topological thinning and bifurcation detection as described in.[18] A rigid 2D-3D registration is computed by distance minimization of 2D and projected 3D centerline curves as has been successfully applied to vessels (see e.g.[5,10]) solving for both a projection matrix and correspondences of centerline points. If corresponding information is not available at each centerline point, a closest point operator can be incorporated after the rigid registration to assign one-to-one correspondences to all curve points. If ambiguities arise in this assignment due to projection overlay of vessel structures, these features can be left out of the correspondence set, which does not influence the proposed method.

*However, any other standard gradient-based approach, such as e.g. Levenberg-Marquardt, can be employed.

†Meaning that intrinsic parameters of the intraoperative imaging device are given. Also, image distortion can be assumed to be absent due to flat-panel detector technology.

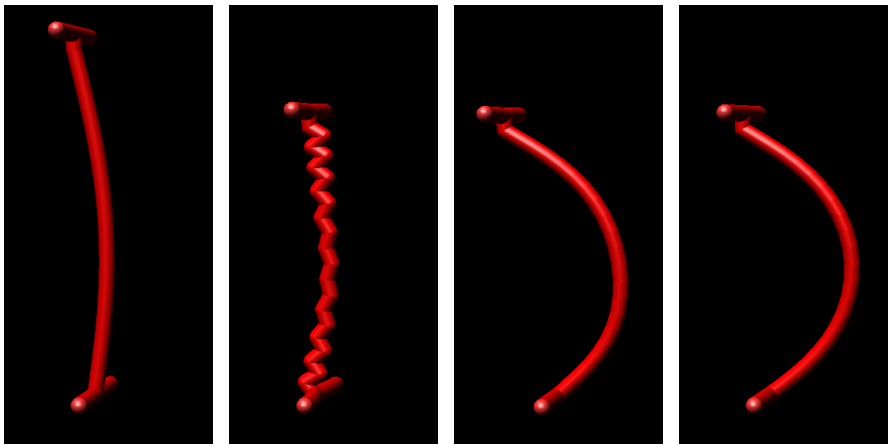

(a) (b) (c) (d)

Figure 4: Demonstrates of the effect of joint usage of the length preservation and the diffusion regularization term. **(a)** Input 3D image. **(b)** Result with Length Preservation. **(c)** Result with Length Preservation and Diffusion Regularization clearly produces a more natural result. **(d)** Ground truth.

### 2.2 Preliminaries and Notation

We model vessel structures as directed graphs $G^d = (V^d, E^d)$, with a set of $n$ nodes $V^d \subset \mathbb{R}^d$ and the connecting edges $E^d \subset V^d \times V^d$. Here $d \in \{2, 3\}$ denotes the dimension of the graph. For the following, please refer also to Figure 5.

The nodes are classified either as bifurcation nodes $V_b^d$ or sampling nodes $V_s^d$, such that $V^d = V_b^d \cup V_s^d$ and $\emptyset = V_b^d \cap V_s^d$ . While the bifurcation nodes express the topology and the rough geometry of the vessel tree, the sampling nodes are used to describe the geometry of the vessel segments in more detail.

The bifurcation nodes are abbreviated by $\mathbf{B}$ and are identified with their spatial coordinates, such that $\mathbf{B} \in V^d$.

We denote the sampling nodes by $\mathbf{X}$ in 3D and $\mathbf{x}$ in 2D and again identify them with their spatial coordinates.

The correspondences between the 3D and 2D points are represented by $C \subset V^3 \times V^2$.

We define a vessel segment $\Pi_{i,j}$ as a path between two neighboring bifurcation nodes $\mathbf{B}_i$ and $\mathbf{B}_j$, containing all sampling nodes and edges between $\mathbf{B}_i$ and $\mathbf{B}_j$. The number of nodes in $\Pi_{i,j}$ is $n_{i,j}$ and the number of edges respectively $n_{i,j} + 1$. The sampling nodes are indexed relative to the vessel segment $\Pi_{i,j}$ starting from 1 to $n_{i,j}$, compare Figure 5. The correspondences are also ordered relative to the respective vessel segment.

The deformation function is encoded by a set of 3D displacement vectors $\varphi \in \mathbb{R}^{3\times n}$ centered in the $n$ graph nodes. The displacement at the $i$-th node $\mathbf{X}_i$ is denoted by $\varphi_i$, such that the final position of the node is $\mathbf{Y}_i = \mathbf{X}_i + \varphi_i$.

We also employ a dense version of the displacement function, which we denote by $\tilde{\varphi}$. We obtain $\tilde{\varphi}$ from $\varphi$ by interpolation using Thin-Plate Splines (TPS).[19] We use the dense displacement field for assigning displacement values to nodes for which no displacement vectors are defined.[‡]

For projections we use a standard pinhole camera model with the principal ray in the direction of the positive Z-axis.

[‡]In order to simplify the implementation, correspondences are computed only for sampling nodes, and thus also the energies are only evaluated there. This technical detail is due to the need to consider predecessor and successor nodes in some parts of the algorithm. In addition, omitting the bifurcation nodes, which often have more than only two neighboring nodes, facilitates the implementation.

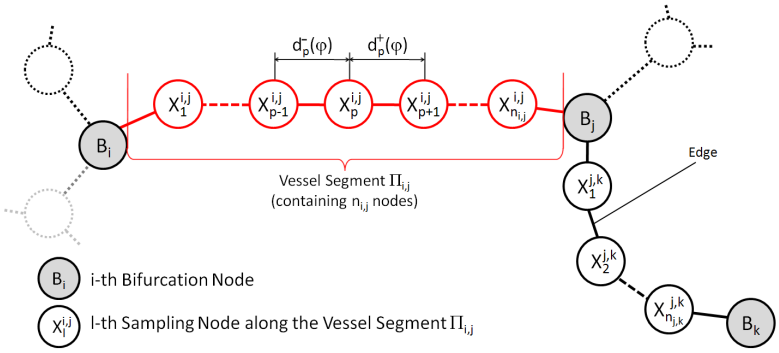


Figure 5: Illustration of the used graph structure.

### 2.3 The Model

The deformable registration process is now described as a minimization of the energy function $\mathcal{E}$ with respect to the displacements $\varphi$ of the vessel nodes in order to get the estimate $\varphi'$ of $\varphi$, that is

$$\varphi' = \arg\min_{\varphi} \mathcal{E} \quad , \tag{1}$$

with the energy function

$$\mathcal{E} = D + \alpha S_L + \beta S_D + \gamma S_P \quad , \tag{2}$$

where $\mathcal{E} : (G^3, G^2, C, \varphi) \mapsto y \in \mathbb{R}$ consists of a difference term $D : (G^3, G^2, C, \varphi) \mapsto y \in \mathbb{R}$ and regularization terms $S_L : (G^3, \varphi) \mapsto y \in \mathbb{R}$ for length preservation of the vessel segments, $S_D : \varphi \mapsto y \in \mathbb{R}$ for smoothness of the displacement field, and the term $S_P : \varphi \mapsto y \in \mathbb{R}$ for retention of initial positions of graph points, which replaces the standard boundary condition. For brevity, we will drop the function arguments in the remainder of the paper. The positive scalars $\alpha$, $\beta$ and $\gamma$ control the influence of the respective terms.

In the following, we present the energy terms from Equation (2). We also give the respective derivatives which are used in the gradient descent optimization scheme.

### 2.4 Difference Measure

The difference measure $D$ which drives the registration process penalizes the distance between the projection of 3D points from the input graph and the corresponding 2D points from the input projection image.

Given point correspondences $C$ with a single correspondence $C_i = (\mathbf{X}_i, \mathbf{x}_i)$ and a projection function $f : \mathbb{R}^3 \to \mathbb{R}^2$, we can define the distance measure

$$D = \frac{1}{n} \sum_{i=1}^{n} \left\| \mathbf{x}_i - f(\mathbf{X}_i + \varphi_i) \right\|^2 \quad . \tag{3}$$

Here, $f : \mathbb{R}^3 \to \mathbb{R}^2$ is a projection function

$$f(\mathbf{X}) = (\mathbf{p}_1^\top \hat{\mathbf{X}} / \mathbf{p}_3^\top \hat{\mathbf{X}}, \mathbf{p}_2^\top \hat{\mathbf{X}} / \mathbf{p}_3^\top \hat{\mathbf{X}})^\top \quad , \tag{4}$$

where $\mathbf{p}_1^\top$, $\mathbf{p}_2^\top$ and $\mathbf{p}_3^\top$ constitute the row vectors of the projection matrix $\mathbf{P} \in \mathbb{R}^{3\times4}$, and $\hat{\mathbf{X}} = [\mathbf{X}^\top, 1]^\top$ is the homogeneous 4-vector of the 3D point $\mathbf{X}$.

For the minimization according to the model (2), the derivative of $D$ with respect to $\varphi_i$ is needed. By using $\mathbf{Y}_i = \mathbf{X}_i + \varphi_i$ the gradient is given by

$$\frac{\partial D}{\partial \varphi_i} = -\frac{2}{n} \left( \mathbf{x}_i - f(\mathbf{Y}_i) \right)^\top \mathbf{J}_i \quad , \tag{5}$$

where $\mathbf{J}_i \in \mathbb{R}^{2\times 3}$ is the Jacobian of $f$ with respect to $\varphi_i$, given by

$$\frac{1}{(\mathbf{p}_3^\top \hat{\mathbf{Y}}_i)^2} \begin{bmatrix} p_{11}\mathbf{p}_3^\top \hat{\mathbf{Y}}_i - p_{31}\mathbf{p}_1^\top \hat{\mathbf{Y}}_i & p_{21}\mathbf{p}_3^\top \hat{\mathbf{Y}}_i - p_{31}\mathbf{p}_2^\top \hat{\mathbf{Y}}_i \\ p_{12}\mathbf{p}_3^\top \hat{\mathbf{Y}}_i - p_{32}\mathbf{p}_1^\top \hat{\mathbf{Y}}_i & p_{22}\mathbf{p}_3^\top \hat{\mathbf{Y}}_i - p_{32}\mathbf{p}_2^\top \hat{\mathbf{Y}}_i \\ p_{13}\mathbf{p}_3^\top \hat{\mathbf{Y}}_i - p_{33}\mathbf{p}_1^\top \hat{\mathbf{Y}}_i & p_{23}\mathbf{p}_3^\top \hat{\mathbf{Y}}_i - p_{33}\mathbf{p}_2^\top \hat{\mathbf{Y}}_i \end{bmatrix}^\top \tag{6}$$

where $p_{ij}$ denote the entries of the projection matrix.

### 2.5 Length Preservation Constraint

Since vessel structures are in general enclosed by soft tissue, for example inside liver, and breathing motion is limited to a certain magnitude, the length change of the vessels is limited. We model this observation by imposing a soft length preservation constraint on the single vessel segments. Thus, we do not impose constant lengths, which would be a too restrictive and unnatural assumption in the given setting. Since the vessel length is defined in 3D space, this constraint is able to induce a deformation orthogonal to projection rays, compare Figure 3a.

We define the terms $d_i^-(\varphi)$ and $d_i^+(\varphi)$, which measure the length of the edges connected to the sampling node $\mathbf{X}_i$ for a given set of displacements $\varphi$ by

$$d_i^-(\varphi) = \|\mathbf{Y}_i - \mathbf{Y}_{i-1}\|^2 \quad , \text{ and} \tag{7}$$

$$d_i^+(\varphi) = \|\mathbf{Y}_i - \mathbf{Y}_{i+1}\|^2 \quad , \tag{8}$$

where we once again set $\mathbf{Y}_i = \mathbf{X}_i + \varphi_i$, compare also Figure 5. Please note that the initial length of the edges connected to $\mathbf{X}_i$ is given by $d_i^-(\mathbf{0})$ and $d_i^+(\mathbf{0})$ where $\mathbf{0}$ is the zero displacement field.

Now we can define a length preserving cost function as

$$S_L = \frac{1}{n}\sum_{i=1}^{n} \left|\frac{d_i^-(\mathbf{0}) - d_i^-(\varphi)}{d_i^-(\mathbf{0})}\right|^2 + \left|\frac{d_i^+(\mathbf{0}) - d_i^+(\varphi)}{d_i^+(\mathbf{0})}\right|^2 \quad , \tag{9}$$

which penalizes the relative deviation from the initial length of the two edges which are directly influenced by the $i$-th node.

The derivative of $S_L$ with respect to $\varphi_i$ reads

$$\frac{\partial S_L}{\partial \varphi_i} = \frac{-8}{n}\left[w_i^-(\mathbf{Y}_i - \mathbf{Y}_{i-1}) + w_i^+(\mathbf{Y}_i - \mathbf{Y}_{i+1})\right]^\top \quad , \tag{10}$$

with $w_i^- = d_i^-(\mathbf{0}) - d_i^-(\varphi)$ and $w_i^+ = d_i^+(\mathbf{0}) - d_i^+(\varphi)$.

The evaluation of the derivative of the length preservation term is performed independently on single vessel segments $\Pi$, since for the computation, ordered correspondences and nodes with a left and right neighbor each are needed.

### 2.6 Diffusion Regularization

The so-called diffusion regularization term is often used in intensity-based registration (compare e.g.[4]) in order to impose a smoothness constraint onto the displacement field. The energy function is defined as

$$S_D = \frac{1}{n}\sum_{i=1}^{n} \left\|\nabla \varphi_i^{(x)}\right\|^2 + \left\|\nabla \varphi_i^{(y)}\right\|^2 + \left\|\nabla \varphi_i^{(z)}\right\|^2 \quad , \tag{11}$$

where $\nabla \varphi^{(d)}$ is defined by using the dense version of the displacement field $\tilde{\varphi}$, which is computed using the 3D Thin-Plate Spline. Here the standard central difference approximation scheme with an appropriate grid spacing $h$ is used.

The derivative of $S_D$ is

$$\frac{\partial S_D}{\partial \varphi_i} = -\frac{2}{n}\Delta\varphi_i = -\frac{2}{n}\left[\Delta\varphi_i^{(x)}, \Delta\varphi_i^{(y)}, \Delta\varphi_i^{(z)}\right] \quad , \tag{12}$$

where $\Delta$ is the Laplace operator with $\Delta\varphi_i^{(d)} = \partial_{xx}\varphi_i^{(d)} + \partial_{yy}\varphi_i^{(d)} + \partial_{zz}\varphi_i^{(d)}$. The Laplace operator is also evaluated by using the dense version of the displacement field.

The evaluation of the TPS for computing the gradient and the Laplacian does not present a large overhead, since the TPS coefficients are already computed in every iteration in order to transform nodes for which no correspondences are defined.

### 2.7 Position Retention Constraint

Instead of using a boundary condition for our problem, such as fixed values for the displacement at certain nodes, we use a soft-constraint which implies that all points should retain their initial position. The advantage of this approach is that it involves no hard constraints, which would possibly require user interaction. The weighting $\gamma$ for the position retention constraint is chosen very low relative to the coefficients for the other terms, such that only the motion along the projection rays is effectively constrained, which is not or hardly constrained by the other terms.

The energy term is defined to minimize the distance between initial and final position as

$$S_P = \frac{1}{n}\sum_{i=1}^{n} \|\mathbf{Y}_i - \mathbf{X}_i\|^2 = \frac{1}{n}\sum_{i=1}^{n} \|\varphi_i\|^2 \quad , \tag{13}$$

and the trivial derivative is

$$\frac{\partial S_P}{\partial \varphi_i} = \frac{2}{n}\ \varphi_i \quad . \tag{14}$$

### 2.8 Optimization Scheme

By using all components of the cost function $\mathcal{E}$ together with their gradients, and the step size $\mu$, we can give an algorithm based on gradient descent optimization:

**Algorithm 1** Deformable 2D-3D Registration with Additional Constraints

Given the input graphs $G^3$ and $G^2$, ordered point correspondences $C_i = (\mathbf{X}_i, \mathbf{x}_i)$,
and a projection matrix $\mathbf{P}$,

**repeat**
  calculate $\nabla\mathcal{E} = \nabla D + \alpha\nabla S_L + \beta\nabla S_D + \gamma\nabla S_P$
  update displacements $\varphi = \varphi - \mu\nabla\epsilon/\|\nabla\mathcal{E}\|$
  update the 3D TPS and deform whole graph
**until** $\|\nabla\mathcal{E}\| < \varepsilon$

In all tests $\alpha$ is approximately 10 times larger than $\beta$, and 100 larger than $\gamma$.

## 3. RESULTS AND EVALUATION

In order to validate our results, besides visual inspection, we compute two different quantitative error measures.

The first is the 3D euclidean distance between the nodes of the ground truth (GT) structure and a given graph.

Since this first measure does not take topology into account we also introduce a second measure, which does not penalize the position, but only evaluates the shape. At every node, the angle between the two adjacent edges is computed.

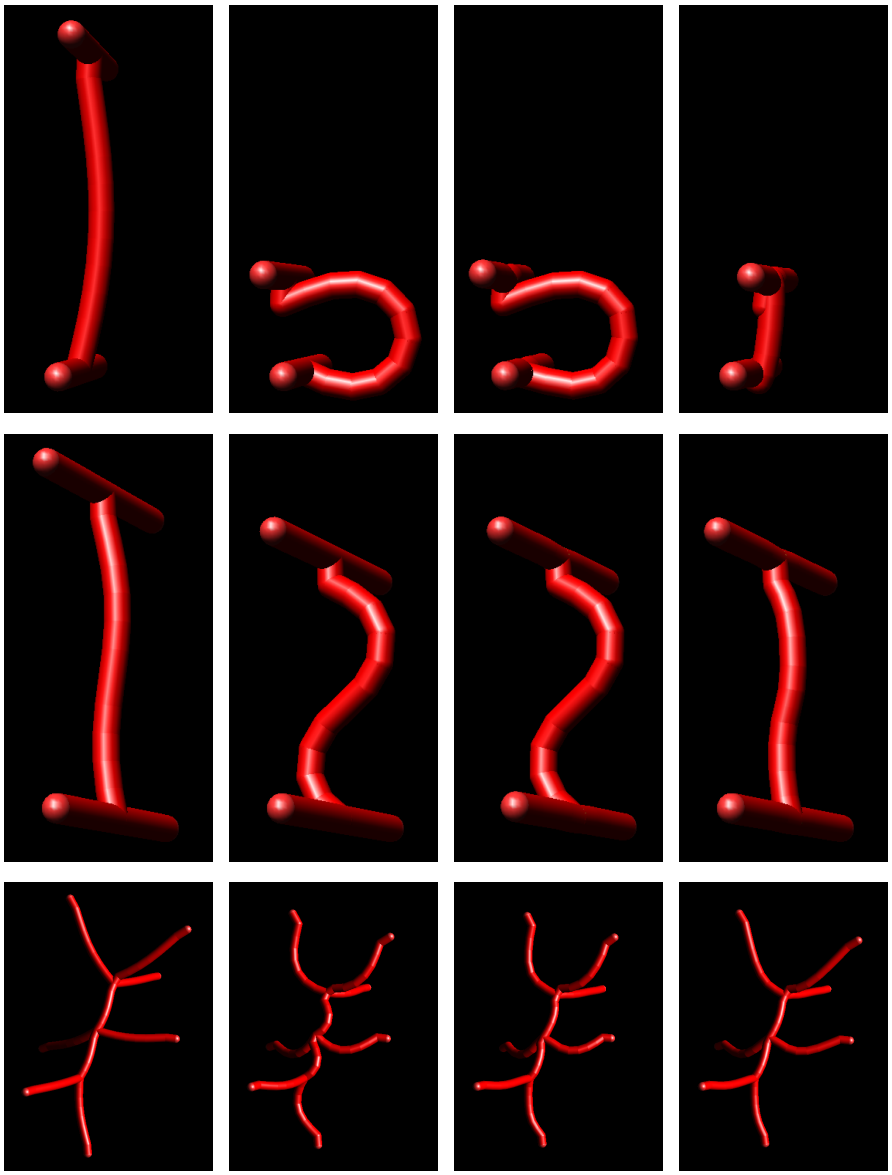

(a) 3D input (b) GT (c) Our method (d) Naive

Figure 6: Visualization of a selection of tests on synthetic data. Every row presents a single example setting, with the quantitative assessment of the results in Table 1 (from top to bottom: Synth 1, Synth 2, Synth 3).

| Test Type | | Position Error [mm] | | Shape Error [rad] | |
|---|---|---|---|---|---|
| **Test** | **Data** | $\mu$ | $\sigma$ | $\mu$ | $\sigma$ |
| Synth 1 | Input | 4.46 | 3.58 | 0.5847 | 0.7769 |
| | Result | 0.19 (95.8%) | 0.05 | 0.0723 (87.6%) | 0.0583 |
| Synth 2 | Input | 1.36 | 1.09 | 0.3224 | 0.3628 |
| | Result | 0.22 (83.5%) | 0.11 | 0.0254 (92.1%) | 0.0192 |
| Synth 3 | Input | 1.42 | 0.80 | 0.3463 | 0.1990 |
| | Result | 0.56 (60.3%) | 0.37 | 0.1503 (56.6%) | 0.1317 |
| Liver 1 | Input | 7.38 | 2.23 | 0.1675 | 0.1676 |
| | Result | 3.25 (56.0%) | 2.89 | 0.1106 (33.9%) | 0.1277 |
| Liver 2 | Input | 1.20 | 0.65 | 0.0082 | 0.0093 |
| | Result | 0.96 (19.7%) | 0.74 | 0.0057 (30.3%) | 0.0075 |

Table 1: Results of error evaluation on several synthetic and real data sets. The position error by euclidean distance, as well as the shape error by angle measurement is assessed. We give the mean error $\mu$ and in order to show the significance of the improvement also the standard deviation $\sigma$. For the mean, the relative improvement to the input data is given in percent. For visualization of the settings, compare Figures 6 and 7.

We perform the tests on synthetic graphs with artificial deformations in order to test various aspects of the method. To demonstrate the applicability for real applications, we apply the tests to real vessels segmented from angiographic images, deformed by both, artificial and natural deformation fields.

The error evaluation is summed up in Table 1. The respective visualization of the results for synthetic data sets is presented in Figure 6. In Figure 7, real data sets together with their extracted vasculature are shown.

### 3.1 Tests on Synthetic Data

For these tests, we generate two 3D graphs by deforming the respective graph structures such that the length is preserved. One of the graphs serves as input for the method, while the other one presents the ground truth solution. The 3D ground truth is not directly used, but we generate a 2D projection of this structure, which is used as input for the method, together with the projection matrix and a correspondence set. For three exemplary data sets (Synth1, Synth2 and Synth3) quantitative and visual results are presented in Table 1 and Figure 6.

### 3.2 Real Data with Artificial Deformation

In order to assess the behavior of the method on natural vessel structures in a quantitative way, we deform the graphs extracted by segmentation from patient data sets with a length-preserving deformation function.[§]This way, we are able to perform our method and measure the distance of the result to a known ground truth in the same way as for synthetic data sets. A projection matrix computed from a rigid CTA-to-DSA registration of the respective patient is used to create the input 2D vessel graph. For the presented tests, we use a liver data set (Liver 1) from a patient who suffers from hepatocellular carcinoma and was treated with Transarterial Chemoembolization, compare Table 1 and Figure 7.

### 3.3 Real Data with Natural Deformation

Natural deformation fields for human organs are hard to obtain. In order to verify our method on possibly natural deformations we employ the results presented by Siebenthal *et al.* [3] The displacement fields provided by this work are computed from a series of contrasted 4D MR images of the liver. A deformable registration is performed in[3] between the single 3D images, while the high time resolution together with the strong texture of the contrasted images assures the quality and reliability of the resulting deformation field. We segment the vessel structures from the contrasted MR images used in,[3] and generate the input 3D graph for our method.

[§]To this end, we employ a dedicated function, which is not used in our method itself, in order to assure the validness of comparison.

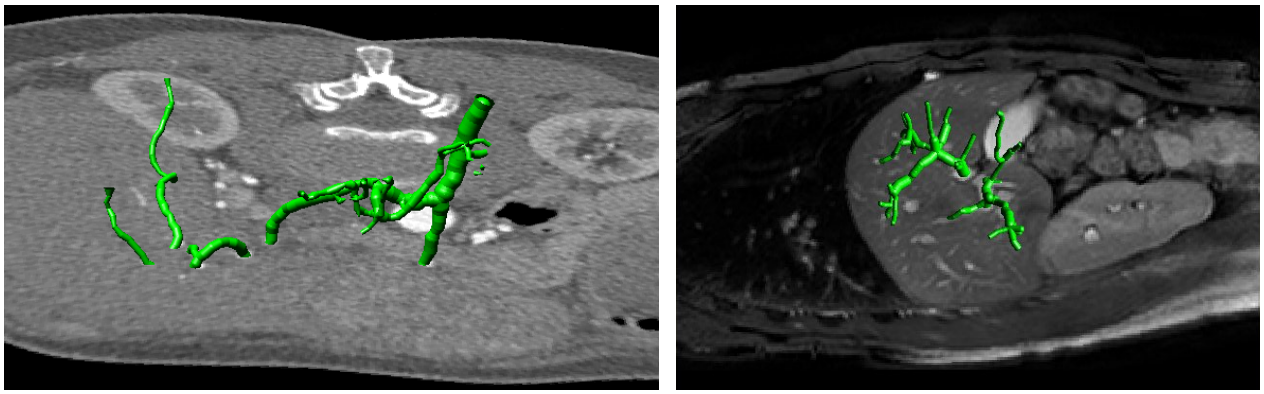

Figure 7: Visualization of segmented real vessel structures. **Left Image:** Liver 1 data set (CTA) taken from a patient suffering from hepatocellular carcinoma. **Right Image:** Liver 2 data set (MRA) taken from Siebenthal *et al.* [3]

Then, we apply the displacement field from[3] to the 3D graph and thus compute the ground truth for the result. A projection matrix yielding an anterior-posterior image was used for 2D input creation. Note that we assure an inherent rigid pre-registration with this setup. In the same way as for the synthetic data sets, the 3D ground truth together with initial and deformed 3D input graph are used to quantitatively assess the performance of our method. Despite the small deformation observable in the data set (Liver 2), a clear improvement is achieved. Compare Table 1 and Figure 7.

## 4. CONCLUSION

In this paper, we present a method for deformable registration of 3D vessel structures to a single 2D projection image. By combining a difference measure with constraints resulting from valid assumptions, we improve the rigid spatial alignment of the 3D vessel, which up to now presents the state of the art for this problem. The improvement in the spatial alignment is important for 3D depth perception and navigation during interventions. Quantitative and qualitative tests on medical and synthetic data sets clearly demonstrate the improvement achieved by our method.

Further work will include improving the optimization methods for the presented model, automatic assessment of the model coefficients, further testing of robustness with respect to missing and wrong correspondences and the actual application of the method in medical settings.

## ACKNOWLEDGMENTS

The authors would like to thank Moritz Blume and Selim Benhimane for discussion and valuable feedback, and Martin Horn for his help with rendering the supplementary material movie.

## REFERENCES

1. S. Aylward and J. Jomier, "Rigid and deformable vasculature-to-image registration: A hierarchical approach," in *MICCAI*, *Lecture Notes in Computer Science* **3216**, pp. 829–836, Springer, 2004.
2. A. Charnoz, V. Agnus, G. Malandain, C. Forest, M. Tajine, and L. Soler, "Liver registration for the follow-up of hepatic tumors," in *MICCAI*, *Lecture Notes in Computer Science* **3750**, pp. 155–162, Springer, 2005.
3. von Siebenthal, M., Szkely, G., Gamper, U., Boesiger, P., Lomax, A., Cattin, and Ph., "4d mr imaging of respiratory organ motion and its variability," *Phys. Med. Biol.* **52**, pp. 1547–1564, February 2007.
4. J. Weickert and C. Schnörr, "A theoretical framework for convex regularizers in pde-based computation of image motion," *International Journal of Computer Vision* **45**(3), pp. 245–264, 2001.

5. J. Feldmar, N. Ayache, and F. Betting, "3D-2D projective registration of free-form curves and surfaces," in *Proc. Int'l Conf. of Computer Vision (ICCV)*, **20-23**, pp. 549–556, IEEE, 1995.
6. J. Hipwell, G. Penney, R. McLaughlin, K. Rhode, P. Summers, T. Cox, J. Byrne, J. Noble, and D. Hawkes, "Intensity based 2D-3D registration of cerebral angiograms," *IEEE Trans. on Medical Imaging (TMI)* **22**, pp. 1417–1426, 2003.
7. H. Chan, A. Chung, S. Yu, and W. Wells, "2D-3D vascular registration between digital subtraction angiographic (DSA) and magnetic resonance angiographic (MRA) images," in *Proc. of the IEEE International Symposium on Biomedical Imaging*, *Lecture Notes in Computer Science* **1205**, pp. 708–711, IEEE, 2004.
8. C. Florin, J. Williams, A. Khamene, and N. Paragios, "Registration of 3D angiographic and X-ray images using sequential monte carlo sampling.," in *Computer Vision for Biomedical Image Applications, First Int'l Workshop, CVBIA '05*, *Lecture Notes in Computer Science* **3765**, pp. 427–436, Springer, 2005.
9. G.-A. Turgeon, G. Lehmann, G. Guiraudon, M. Drangova, D. Holdsworth, and T. Peters, "2D-3D registration of coronary angiograms for cardiac procedure planning and guidance," *Medical Physics* **32**, pp. 3737–3749, 2005.
10. M. Groher, N. Padoy, T. Jakobs, and N. Navab, "New CTA protocol and 2D-3D registration method for liver catheterization," in *MICCAI*, *Lecture Notes in Computer Science* **4190**, pp. 873–882, 2006.
11. J. Jomier, E. Bullitt, M. van Horn, C. Pathak, and S. Aylward, "3d/2d model-to-image registration applied to tips surgery," in *MICCAI*, pp. 662–670, 2006.
12. M. Fleute and S. Lavallee, "Nonrigid 3-d/2-d registration of images using statistical models," in *MICCAI*, pp. 138–147, Springer, (London, UK), 1999.
13. S. Benameur, M. Mignotte, S. Parent, H. Labelle, W. Skalli, and J. de Guise, "3d/2d registration and segmentation of scoliotic vertebra using statistical models," *Computerized Medical Imaging and Graphics* **27**, pp. 321–337, 2003.
14. J. Yao and R. Taylor, "Assessing accuracy factors in deformable 2d/3d medical image registration using a statistical pelvis model," in *Proc. Int'l Conf. of Computer Vision (ICCV)*, p. 1329, IEEE Computer Society, (Washington, DC, USA), 2003.
15. G. Zheng, "A novel 3D/2D correspondence building method for anatomy-based registration," in *3rd Int'l. Workshop on Biomedical Image Registration*, pp. 75–82, Springer, 2006.
16. T. S. Y. Tang and R. E. Ellis, "2d/3d deformable registration using a hybrid atlas," in *MICCAI*, *Lecture Notes in Computer Science* **3750**, pp. 223–230, Springer, 2005.
17. K. Grochow, S. L. Martin, A. Hertzmann, and Z. Popovic, "Style-based inverse kinematics," in *ACM Transactions on Graphics (Proc. of SIGGRAPH 2004)*, 2004.
18. D. Selle, B. Preim, A. Schenk, and H.-O. Peitgen, "Analysis of vasculature for liver surgery planning," *IEEE Trans. on Medical Imaging (TMI)* **21**(8), pp. 1344–1357, 2002.
19. G. Wahba, *Spline Models for Observational Data (C B M S - N S F Regional Conference Series in Applied Mathematics)*, Society for Industrial & Applied Mathematics, 1990.